Journal of
Marine Science and Engineering

MDPI

Article

Structural Influence of the Cargo Holds of a 3000 m^3 Wellboat on a Double-Bottom Floor

Arturo Silva-Campillo * and Francisco Pérez-Arribas

Department of Naval Architecture, Shipbuilding and Ocean Engineering, Universidad Politécnica de Madrid (UPM), Avenida de la Memoria SN, 28040 Madrid, Spain; francisco.perez.arribas@upm.es
* Correspondence: a.silva@upm.es

Abstract: In order to reduce weight and facilitate maintenance, servicing and inspection, ship structures usually have openings and cutouts. However, these modifications frequently weaken the plates' ability to buckle. In this work, the combined effects of geometric discontinuities (such as openings and cutouts) under diverse in-plane loads (such as horizontal compression, vertical compression, biaxial compression, and in-plane edge shear loading) are taken into consideration as the perforated plates located in the double-bottom floor of a 3000 m^3 wellboat are investigated for their linear and elastic buckling behavior. In order to assess the effects of various stiffening methods and their interactions with different load scenarios, as well as fluctuating plate slenderness ratios, the research combines experimental and numerical analyses. This thorough study identifies the best stiffening technique and suggests alternative geometries that minimize structural weight through topology optimization. The research's findings are helpful in comprehending the mechanisms underlying structural failure and in offering design and recommendation guidelines that enhance hull inspections and the assessment of structural flaws.

Keywords: ship floor; cutout; buckling strength; opening

Citation: Silva-Campillo, A.; Pérez-Arribas, F. Structural Influence of the Cargo Holds of a 3000 m^3 Wellboat on a Double-Bottom Floor. *J. Mar. Sci. Eng.* **2024**, *12*, 994. https://doi.org/10.3390/jmse12060994

Academic Editors: Baiqiao Chen, Sheng Xu and Emre Uzunoglu

Received: 22 May 2024
Revised: 10 June 2024
Accepted: 11 June 2024
Published: 14 June 2024

1. Introduction

A wellboat is an innovative vessel designed for the live transportation of fish and plays a pivotal role in the aquaculture industry and the preservation of fish quality. The nomenclature 'wellboat' stems from the amalgamation of 'well' and 'boat,' underscoring its most distinctive feature: the presence of compartments or wells that are filled with seawater. This characteristic enables the creation of an ideal aquatic environment for keeping live fish during transit, reducing stress and potential harm. Wellboats are outfitted with water recirculation systems and temperature controls, ensuring that fish arrive at markets or processing facilities in excellent condition, thereby improving the freshness and quality of the final product. The most notable feature of these vessels is their cargo holds, which play a central role in transporting live fish. These holds are specifically designed to maintain optimal conditions during transit, with advanced water recirculation systems and temperature controls that minimize stress and preserve fish health. Additionally, they prevent contamination of the surrounding water by fish waste, facilitate the segregation and classification of different fish batches according to their handling needs, and ensure the safety of onboard personnel when working with live fish. As a result, wellboats are essential for the successful transport of live fish.

Because wellboats have a special structural design with longitudinal framing and double bottoms, it is crucial to assess their structural integrity [1]. The transverse elements of the double-bottom structure, referred to as floors, are essential. These floors have multiple openings for pipe passage, inspection, or weight reduction in addition to cutouts for bottom and double-bottom stiffeners. These characteristics work together to impact the floor's structural capacity and produce stress concentration areas [2]. In order to assess the

floor's structural integrity, it must be analyzed as a set of plates or stiffened panels with cutouts and openings. These features naturally lower the plate's buckling strength and must be taken into account when designing the structural panels. The distinctive structural design of wellboats is typified by their double bottom. Many studies have been conducted on this kind of structure and have looked at different aspects. For instance, Wang et al. [3] studied the relevant behavior, including buckling and ultimate strength, through linear and non-linear and finite element method (FEM) analyses. They took geometric parameters into consideration and suggested a simplified formula to incorporate reduction factors. Furthermore, by examining the effects of small and large openings on maximum stress through numerical and experimental studies, Liu et al. [4] offered useful insights. They specifically focused on longitudinal and transverse girders under combined uniaxial and lateral loads on deck panels.

According to Saad-Eldeen et al. [5], who investigated the effects of different opening dimensions found that forms, steel components, the presence or lack of structural frameworks on the maximum load strength of steel plates under test results, stiffeners, and the configuration of openings are crucial to a structural evaluation. In a similar vein, Yanli et al. [6] investigated how opening attributes like size, shape, and position affect the buckling strength. Building on this, Saad-Eldeen et al. [7] conducted a series of experimental tests on various high-strength steels under uniaxial compressive loads to explore the influence of opening shape (circular and enlarged circular) and size. Given the nature of this structural feature, adequate reinforcement is essential to preserving integrity over the course of its useful life. As a result, this problem has been the subject of many studies. For instance, the investigation of Kim et al. [8] into the best reinforcing methods by which to increase perforated plate buckling and ultimate strength resulted in the creation of a design method for these computations.

The influence of corrosion is another important consideration in the analysis of this type of structure. Chichi and Garbatov [9] have investigated how well a double-bottom side girder plate impacted by corrosion could be made structurally strong again. They examined a side girder with a manhole-shaped opening that was randomly and non-uniformly corroded while it was subjected to uniaxial compressive loads. Similar to this, Cui and Wang [10] used both experimental and numerical methods to study the compressive ultimate strength of traditional stiffened plates with holes susceptible to corrosion of the perforation type. Saad-Edeen et al. [11] examined motion interactions, dissipated energy, strength–strain endurance, durability and failure modes in determining the ultimate strength of steel plates with a large central elongated circular opening under uniaxial compressive loads.

The impact of unconventional geometries has also been examined; Saad-Eldeen et al. [12] evaluated the residual structural performance of steel plates with and without locked cracks and a large central ellipsoidal opening. The behavior of unstiffened plates with rectangular openings under different circumstances, including plate slenderness, opening area ratio, and opening position ratio, was investigated by Yu and Lee [13]. In their investigation of the post-peak behavior under axial and out-of-plane loads, Kumar et al. [14] used finite element (FE) analysis to study the behavior of stiffened plates with angle sections and square openings up to collapse. Li et al. [15] examined the mechanical behavior of common composite structures with fully accessible holes while taking alternative materials into consideration. Doan et al. [16], who examined and contrasted the ultimate compressive strength of comparable aluminum- and steel-stiffened panels, demonstrated that initial deformations, boundary conditions, and the existence of openings on the web of longitudinal girders are among the factors that greatly influence structural determination.

An appropriate set of boundary conditions is necessary for structural analysis. Using finite element (FE) codes, Xu et al. [17] investigated the effects of model geometry and boundary conditions on the anticipated collapse behavior of stiffened panels. The behavior of such openings is often analyzed using finite element analysis (FEA). Through mechanical

testing and nonlinear FEA, Kim et al. [18] conducted both experimental and numerical investigations to ascertain the buckling and maximum strength of plates and stiffened panels under the presence of openings for axial loading. Similarly, Cui and Wang [19] used nonlinear finite element analysis to investigate the maximum strength of standard longitudinal girders that were subjected to longitudinal compression and had openings within the double bottom. Due to either vertical or horizontal hull girder bending moments in ships, Paik [20] investigated the ultimate strength of steel plates under the presence of a single circular hole for axial loading along short edges. ANSYS 2023 software was used in this study to modify parameters like plate characteristics (aspect ratio and thickness) and hole size.

In order to determine the ideal geometry for fatigue strength evaluation, Silva-Campillo et al. [21] looked into how the radius of curvature in different cutout geometric shapes inside the transverse web frame impacts the facilities of longitudinal stiffeners. By using finite element-based shape optimization to reduce stress concentrations and create an optimized cutout shape, Andersen [22] introduced a novel fatigue-resistant cutout design. Furthermore, Silva-Campillo et al. [23] investigated the impact of every cutout in the torsion box's primary transverse structure, especially those related to longitudinal stiffeners. A non-linear multivariable optimal solution tool was used in this analysis to maximize the structure's local weight.

This investigation focuses on analyzing a perforated plate, representing the double-bottom floor of a wellboat, with opening and cutouts. The study evaluates the elastic buckling strength under various combinations of load conditions, stiffening methods, and geometrical characteristics. The paper is structured as follows: a theoretical background (Section 2) provides the theoretical foundation for the linear eigenvalue buckling analysis, case study establishment (Section 3), where geometric models, stiffening methods, and descriptions of the testing machine are outlined to establish the case study. Finite element method and validation (Section 4) defines the finite element method and presents the validation procedure to ensure consistency between numerical and experimental models. A results analysis (Section 5) focuses on stress states and buckling strength assessment. Different geometrical design alternatives and load conditions are compared to derive meaningful insights. Finally, the conclusion (Section 6) provides conclusions drawn from the results obtained in the preceding sections, summarizing the key findings and implications of the study.

2. Analysis of Buckling Eigenvalues in a Linear Framework

The concept of linear tensile buckling is framed as an eigenvalue problem, where eigenvalues denote the loads leading to buckling, and eigenvectors portray the specific buckling patterns [24].

$$([K] - \lambda_i[S])\{\Psi\}_i = \{0\} \tag{1}$$

In the previous equation, $[K]$ denotes the stiffness matrix, $[S]$ represents the stress stiffness matrix, λ_i signifies the ith eigenvalue buckling factor used for scaling the generated loads and Ψ_i. The equation dictating the behavior of the buckled and intact plate subjected to uniaxial compression conditions is formulated as follows by means of Kirchoff plate formulation based on the Sophie–Germain isotropic plate equation under rectangular geometry and simple supported edges conditions [24]:

$$\frac{\partial^4 w}{\partial x^4} + \frac{2\partial^4 w}{\partial x^2 \partial y^2} + \frac{\partial^4 w}{\partial y^4} = \frac{12(1-\nu^2)}{Et^3}\left(-N_x \frac{\partial^2 w}{\partial x^2}\right) \tag{2}$$

In the previous equation, ν stands Poisson's ratio, N_X represents the in-plane loading, t refers to the plate thickness, E represents the Young's modulus and w indicates in the z-direction the vertical deflection of a point located in the (x, y) plate mid plane. In the

scenario of a plate simply supported on all edges, this deflection can be approximated as follows [24]:

$$w = \sum_{m=1}^{\infty} \sum_{n=1}^{\infty} A_{mn} \sin \frac{m\pi x}{a} \sin \frac{n\pi y}{b} \tag{3}$$

In this scenario, m and n symbolize the number of half waves in the x and y direction (as the local axes aligned with and perpendicular to its long edge, respectively). On the other hand, a and b denote the dimensions of the plate in both directions. Following the boundary conditions, a nontrivial solution is obtained as follows [24]:

$$A_{mn}\left[\pi^4\left(\frac{m^2}{a^2}+\frac{n^2}{b^2}\right)^2 - \frac{N_x}{D}\frac{m^2\pi^2}{a^2}\right] = 0 \tag{4}$$

where $N_x = \frac{k\pi^2 D}{b^2}$, $D = \frac{Et^3}{12(1-\nu^2)}$ is the plate stiffness, $k = \left(\frac{m}{\alpha}+\frac{\alpha}{m}\right)^2$ is the factor that takes buckling into account and $\alpha = {}^{a}/_{b}$ denotes aspect ratio. In a uniaxial compression regime, the critical buckling stress under elastic conditions σ_{buck} is a widely recognized formula [25].

$$\sigma_{buck} = \frac{k\pi^2 E}{12(1-\nu^2)}\left(\frac{t}{b}\right)^2 \tag{5}$$

The buckling strength under elastic conditions and a plasticity correction, with the Johnson–Ostenfeld formula [25], is evaluated to obtain the critical buckling strength.

$$\sigma_{cr} = \begin{cases} \sigma_{buck} \\ \sigma_y\left(1-\frac{\sigma_y}{4\sigma_{buck}}\right) \end{cases} \text{for } \sigma_{cr} = \begin{cases} \sigma_{buck} \\ \sigma_y\left(1-\frac{\sigma_y}{4\sigma_{buck}}\right) \end{cases} \tag{6}$$

where σ_y denotes the yield stress, σ_{cr} is the critical buckling stress and p_r is a coefficient that considers the sensitivity to plasticity, typically falling within the range of 0.5 to 0.6. A shearing load can induce buckling by generating in-plane compressive stress. In the scenario of pure shear, the in-plane compressive stress operates at a 45-degree angle with respect to the shear axis [26].

$$\tau_{cr} = \frac{k\pi^2 E}{12(1-\nu^2)}\left(\frac{t}{b}\right)^2 \text{ with } \begin{cases} k = 5.34 + \frac{4}{\alpha^2} & \text{for } \alpha > 1 \\ k = \frac{5.34}{\alpha^2} + 4 & \text{for } \alpha \le 1 \end{cases} \tag{7}$$

An analytical method by which to elucidate the elastic buckling characteristics of a plate simply supported under different applied stress components is outlined as follows [25]:

$$\left(\frac{\sigma_x}{\sigma_{xu}}\right)^{c_1} + \beta\left(\frac{\sigma_x}{\sigma_{xu}}\right)\left(\frac{\sigma_y}{\sigma_{yu}}\right) + \left(\frac{\sigma_y}{\sigma_{yu}}\right)^{c_2} + \left(\frac{\tau}{\tau_u}\right)^{c_3} = 1 \tag{8}$$

where σ_{yu}, τ_u and σ_{xu} are the ultimate strengths under axial loading; σ_x, σ_y and τ are the axial stress in the x-direction, in the y-direction and edge shear, respectively; and c_1, c_2, c_3 and β are factors depending on load and boundary conditions. Equation (9), for biaxial compressive loading, reduces to

$$\left(\frac{\sigma_x}{\sigma_{xu}}\right)^2 + \left(\frac{\sigma_y}{\sigma_{yu}}\right)^2 = 1 \tag{9}$$

An alternative formulation to describe biaxial compression of the plate is presented by Paik [26].

$$\frac{m^2}{a^2}\sigma_x + \frac{n^2}{b^2}\sigma_y - \frac{\pi^2 D}{t}\left(\frac{m^2}{a^2}+\frac{n^2}{b^2}\right)^2 = 0 \tag{10}$$

3. Case Study

3.1. Description

The general overview of the 3000 m^3 wellboat is shown in Figure 1, with the following deck distribution: tank deck at 6400 mm, main deck at 7650 mm, shelter deck at 10,350 mm, forecastle deck at 13,050 mm, navigation bridge deck at 16,050 mm and top of wheelhouse at 18,650 mm. All decks are measured relative to the baseline.

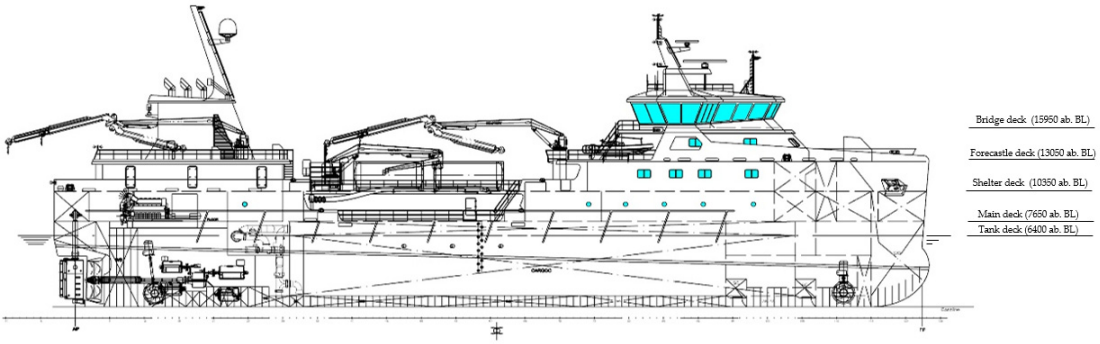

Figure 1. General arrangement of the 3000 m^3 wellboat.

A 3000 m^3 wellboat is selected with its main particulars as follows in Table 1.

Table 1. Main particulars.

Description	Unit	Value
Scantling length (L)	m	73.4
Breadth moulded (B)	m	16
Max. service speed (V)	kn	13
Depth at shelter deck (D_1)	m	10.35
Depth at forecastle deck (D_2)	m	13.05
Scantling draught (T)	m	6.8
Transverse structure spacing (S)	m	2.4

The material characteristics for the selected standard grade A steel (AH24), commonly employed in shipyards, are detailed in Table 2.

Table 2. Material characteristics.

Elastic Modulus, E (GPa)	Yield Stress, σ_{yield} (MPa)	Shear Yield Stress, τ_{yield} (N/mm^2)	Poisson Ratio, v	Density, ρ (ton/m^3)
206	235	181.9	0.3	7.85

The vessel has three independent cargo tanks, separated by two longitudinal bulkheads, a double bottom and a double hull, and these are sized to withstand an overpressure of 0.5 bar and a vacuum pressure of 0.3 bar, accessed through hatches located on the main deck (Figure 2).

Inside the three tanks, movable bulkheads are arranged to displace the fish during the unloading operation (Figure 3). It is ensured that there are no areas within the tank where water does not circulate, thus guaranteeing minimal mortality of the transported fish and ensuring that that they reach their destination in optimal condition.

(**a**) (**b**)

Figure 2. Access to cargo tanks from main deck. (**a**) Exterior view, (**b**) interior view.

(**a**) (**b**)

Figure 3. Interior of the cargo tanks and transverse bulkhead arrangement to facilitate unloading operations. (**a**) port tank, (**b**) starboard tank.

The tanks are designed for seawater circulation, either internally or with inlet and outlet from/to the sea. They are equipped to perform water treatment. After use, each tank is disinfected by ozone injection. A vacuum system is used to load and unload fish and prevent any damage to them. The loading tanks have an automatic cleaning system, as well as water circulation channels and filling and emptying systems through special bottom valves.

Figure 4 shows the particularized block drawing for the double-bottom area of the ship's midbody along with the construction process of those blocks.

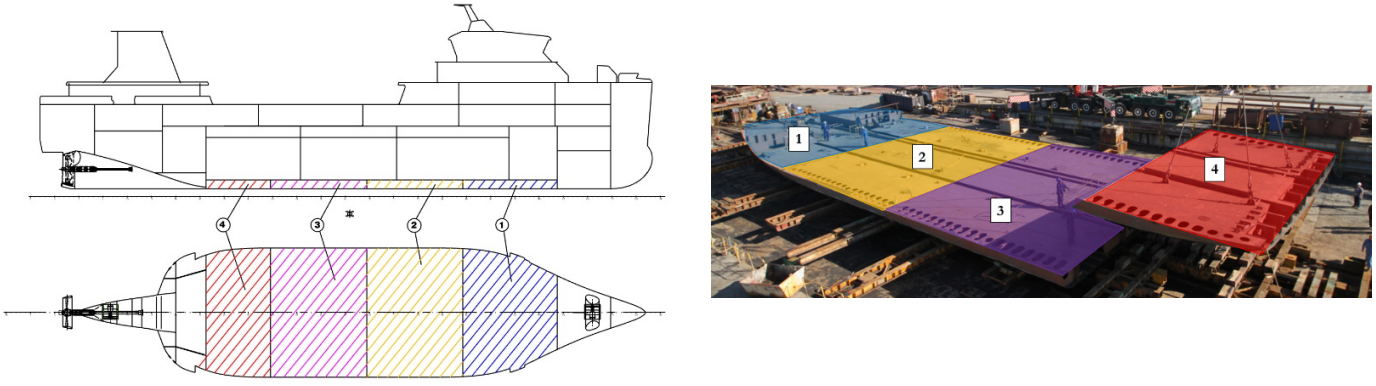

(**a**) (**b**)

Figure 4. (**a**) General view of double-bottom tanks and (**b**) construction process of double-bottom tanks.

With small deflections, a linear elastic material response is assumed. The height of the ship's floor is equal to its double-bottom height (h_w) and equal to 1900 mm, divided by the length of its longitudinal girders (l_w) and equal to 2487 mm, divided by the length of its longitudinal stiffeners (s) and equal to 829 mm and its thickness of 10 mm. The study area is between two longitudinal girders, indicated by four cutouts for standard stiffeners (bulb profile, HP) to pass through. The stiffeners are designed to be as compact as possible, with smooth, rounded edges, as shown in Figure 5, and an elongated central opening ($f_1 = f_2$) of standard dimensions (h_h and b_h) and 600 × 400 mm (with a smoothly curved design, R).

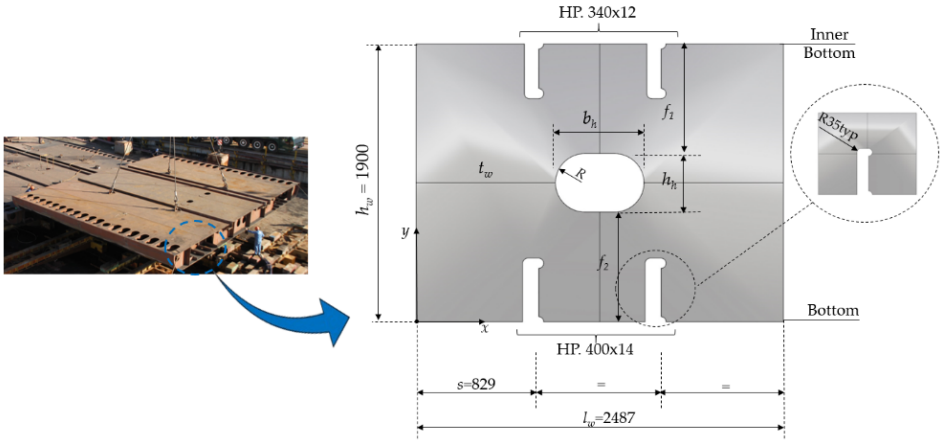

Figure 5. Nomenclature and dimensions of double-bottom floor located in block 3.

The process for preparing test specimens, scaled up by a factor of six and utilizing the material properties outlined in Table 2, involves the following several stages: placing the first markings on the surface, cutting with air plasma, utilizing flat and round steel files for refining, a surface treatment that includes an initial acetone cleaning, white contrast paint application, and then indirect black paint spraying to produce an irregular mesh configuration for digital image correlation (DIC) analysis (Figure 6).

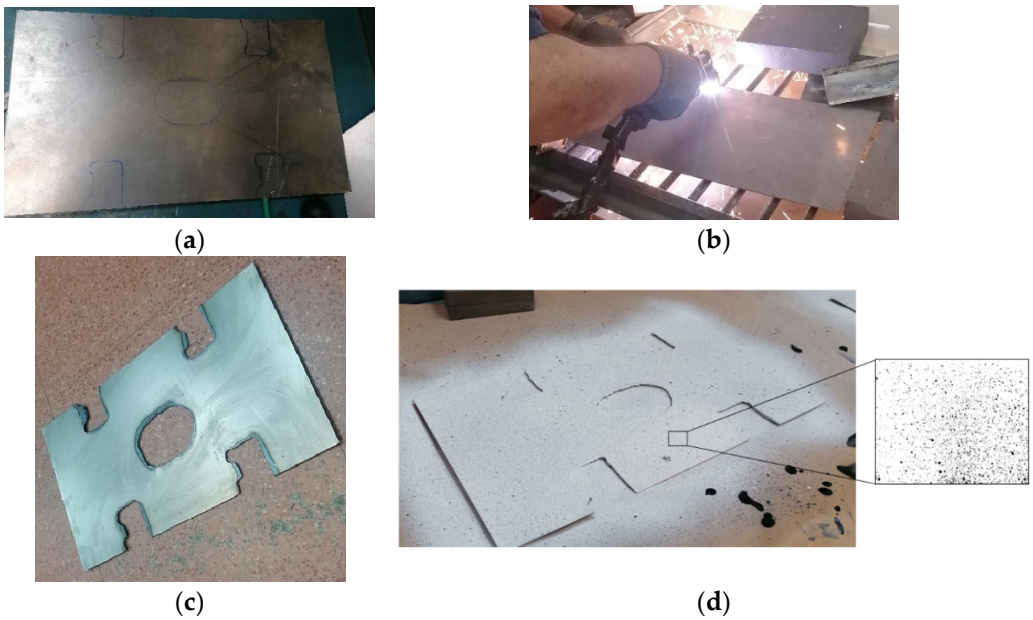

Figure 6. Test specimen preparation procedure. (**a**) Marking of plates, (**b**) cutting procedure, (**c**) specimen testing and (**d**) painting and random meshing.

The analysis model is equipped with web stiffeners (flat bar type) to strengthen the central opening in accordance with the arrangements and solutions depicted in Figure 7 [27].

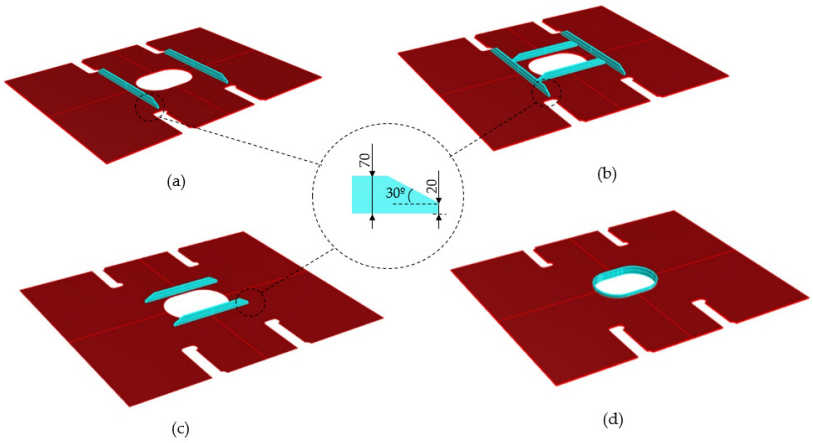

Figure 7. Structural configurations of stiffening techniques include the following: (**a**) two upright flat face plates, (**b**) a combination of two horizontal and two vertical straight face plates, (**c**) two flat horizontal face plates and (**d**) one face plate surround central opening.

Cases (a) and (b) illustrate the vertical face plate placement in regard to the longitudinal stiffeners, case (c) is the same as case (b) but without the vertical face plates, and case (d) shows the horizontal face plate spacing from the opening's end (20 mm). Case (d) is a constant face plate with edge stiffening inside the opening. The flat bars of cases (a), (b), and (c) are sniped at both edges at an angle of 30° in accordance with the protocol recommended by the classification society Det Norske Veritas [28] (Figure 7). Their initial dimensions of 70 × 10 mm are all the same, as reported by Senjanovic et al. [29]. The geometric parameters that are taken into account are the stiffening method (a, b, c, and d), the different face plate scantlings and the slenderness ratio $\left(\lambda = {}^{b}/_{t}\sqrt{{}^{\sigma_{yield}}/_{E}}\right)$ in relation to different plate thickness t values, where b is a set factor that indicates the shortest side of the plate. The straight face plates with sniped ends are prepared with the same parametric scale factor as the perforated plate (Figure 8).

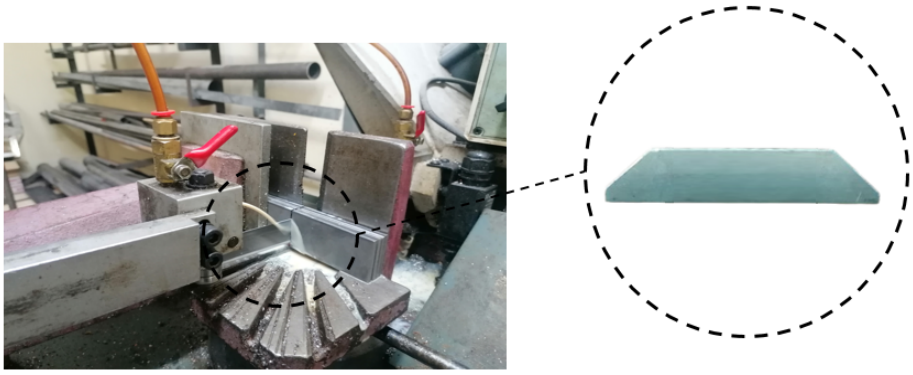

Figure 8. Procedure for preparing straight face plates with sniped ends.

Depending on the stiffening technique, Figure 9 shows the metal active gas (MAG) weld joining procedure for every test specimen.

This study assumes almost perfect workmanship and does not consider the effect of welding and, therefore, the residual stresses and strains.

(**a**) (**b**)

Figure 9. Welding procedure. (**a**) Combination of two horizontal and two vertical straight face plates and (**b**) two upright flat face plates.

3.2. Loading and Boundary Conditions

The double-bottom floor under study is considered to be located under the central cargo tank, which is under a quasi-static loading regime, subject to vertical and horizontal acceleration of the ship as a consequence of the standard mass of water in the tank and in addition to the equivalent design wave pressure of the water acting on the hull (Figure 10).

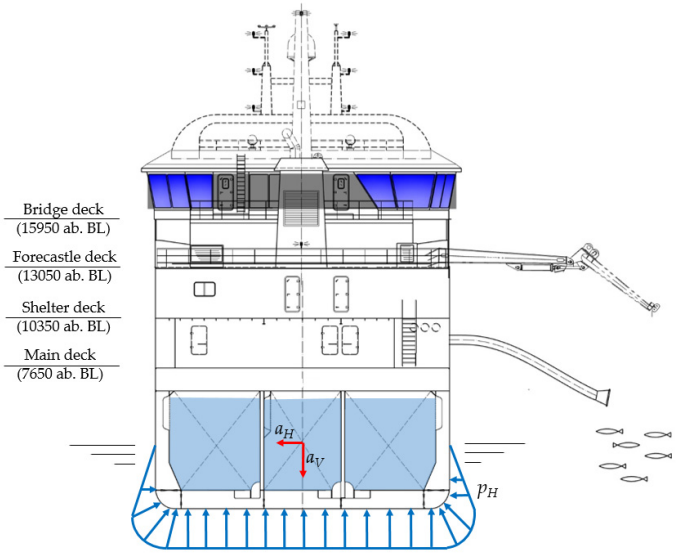

Figure 10. Cross-sectional arrangement of tanks and loading conditions on the double-bottom floor.

The influence of ship motions on a vessel's forces is significant and necessitates their inclusion in calculations [30]. Neglecting to account for these motions can lead to severe consequences, affecting the stability, structural integrity, and material responses of the ship. The transverse acceleration due to sway, in m/s^2, is to be taken from the following [31]:

$$a_{sway} = \frac{115 f_R f_S f_{nl} H}{L f_{TL}^{0.15} f_{BL}^{0.5}} \tag{11}$$

where H is the wave parameter with unrestricted navigation under a strength assessment condition, f_R is the routing factor, f_S is the speed effect coefficient, f_{TL} is the ratio between draught at the considered loading condition and rule length and f_{BL} is the ratio between molded breadth and rule length [31]. The vertical acceleration due to heave, in m/s^2, is to be taken as follows:

$$a_{heave} = \frac{350 f_R f_S f_{nl} H}{L f_{BL}^{0.5}} \tag{12}$$

The summary of accelerations influencing the design of the double-bottom floor is shown in Table 3.

Table 3. Acceleration values.

Movement	Value (m/s^2)
Sway	3.77
Heave	4.86

The wellboat's righting and heeling conditions are compared based on the acceleration values mentioned above. The floor plate is considered to be simply supported on all edges, and the loading conditions on the double-bottom floor are estimated using the Aalbers Ship Design B. V. procedure [32], with a standard heel angle of 20°. The resultant load is a 10 kN trial test load, which includes biaxial compression, in-plane edge shear loading, longitudinal compression, and loading over short edges (Figure 11).

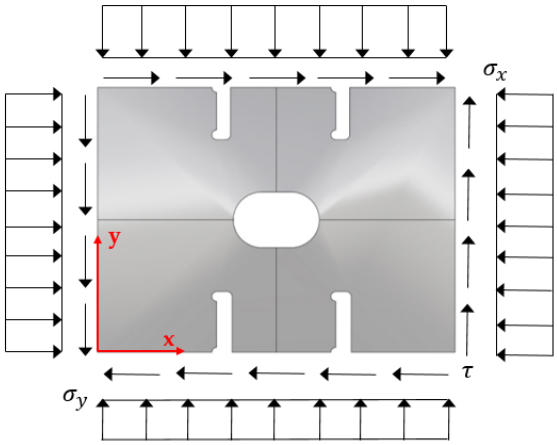

Figure 11. Loading scenarios.

In practical engineering, adopting a simply supported condition is useful because it yields more conservative results than the clamped condition [33]. A total of 324 possible cases are examined, based on the load conditions that have been established and the geometrical considerations discussed in the previous section. Table 4 summarizes the combinations that are examined.

Table 4. Combinations of loads and geometrical parameters.

Method	Stiffening Dimensions (in mm)		Description	Slenderness Ratio	Loading Condition
a, *b*, *c* or *d*	70	10	β 70 × 10	Via plate thickness: 10, 12 or 14 mm	In-plane edge shear loading, biaxial compression, transverse compression and longitudinal compression
		12	β 70 × 12		
		14	β 70 × 14		
	80	10	β 80 × 10		
		12	β 80 × 12		
		14	β 80 × 14		
	90	10	β 90 × 10		
		12	β 90 × 12		
		14	β 90 × 14		

β denotes the stiffening method. The specimen is installed in the testing machine using the upper transition block, a U-shaped piece fixed at the bottom in the lower clamping that is screwed onto a cylindrical component to replicate the imposed loads (Figure 12).

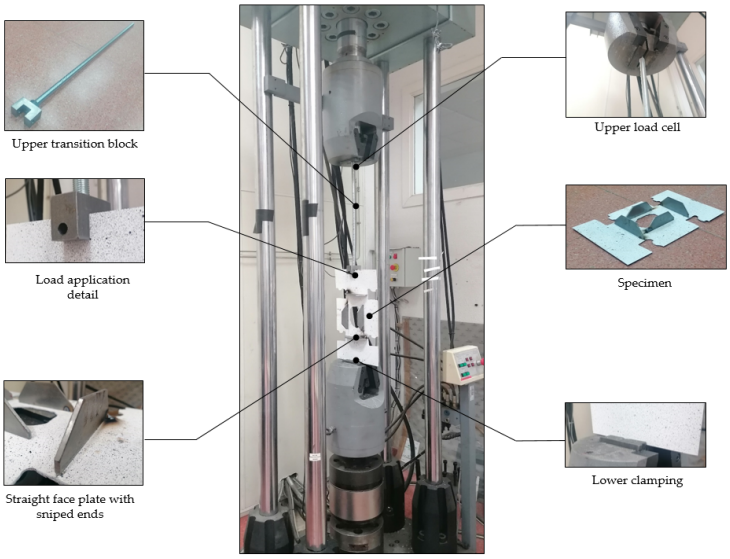

Figure 12. Experimental test arrangement (Servosis INSTRON® 500 kN 2513-501).

4. Methodology

A linear elastic material behavior with a small deflection theory is assumed at this early stage of research. The evaluation of buckling strength is carried out using the commercial program ANSYS® Workbench 2024, which includes a variety of 3D solid finite elements and tetrahedral elements for the analysis of stresses along the thickness to determine the fine mesh size; this results in a reasonably seamless transition between the various model regions [8]. The finite element model is displayed in Figure 13.

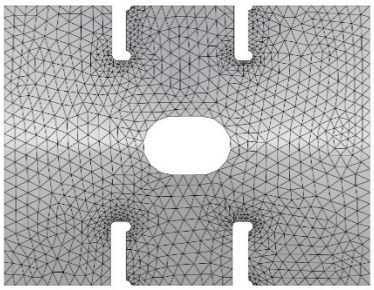

Figure 13. Mesh pattern.

The numerical model, for the particular case of the unstiffened perforated plate, has 32,212 nodes and 15,330 elements.

4.1. Process of Mesh Convergence

The precision and dependability of the outcomes are evaluated using a suggested two-stage verification analysis. In the first, a mesh convergence process was discovered for the unstiffened plate by iteratively adjusting the solution number until the von Mises stress (σ_{VM}) changed between two successive values in a way that was near the shorter of the finite element reliability considerations used by Patil and Jeyakarthikeyan [34]. Table 5 shows the mesh's convergence rate as a function of the elements and nodes used, with an average element edge length of 48.798 mm. Combining 22,324 elements and 46,599 nodes results in a workable solution (with an alteration of 0.72% at a lower processing).

Table 5. Iteration procedure for mesh convergence.

Iteration Step	σ_{VM} (MPa)	Change (%)	Elements	Nodes
1	1.9	-	1705	3742
2	2.45	26.22	5739	12,332
3	2.93	16.58	15,331	32,213
4	3.13	0.72	22,324	46,599

4.2. Validation Study

The agreement between the numerical and experimental regimes in view of high deformation is shown in Table 6.

Table 6. Maximum deformation (mm) according to stiffening method between experimental and numerical fields.

Stiffening Method	Numerical Results	Experimental Results	Difference between Numerical and Experimental Results (%)
a	0.156	0.15	3.84
b	0.135	0.14	3.57
c	0.174	0.18	3.33
d	0.171	0.16	3.61
None	0.184	0.19	3.15

In order to conduct a confirmation study on a plate with an extended circular opening, the outcomes of several analytical formulations are compared with the FEM results in the second step. To this end, the elongated circular opening (Figure 14) is compared with the simple circular opening (R = 265 mm), which keeps the same maximum stress, with a fluctuation of 0.55% between these geometries.

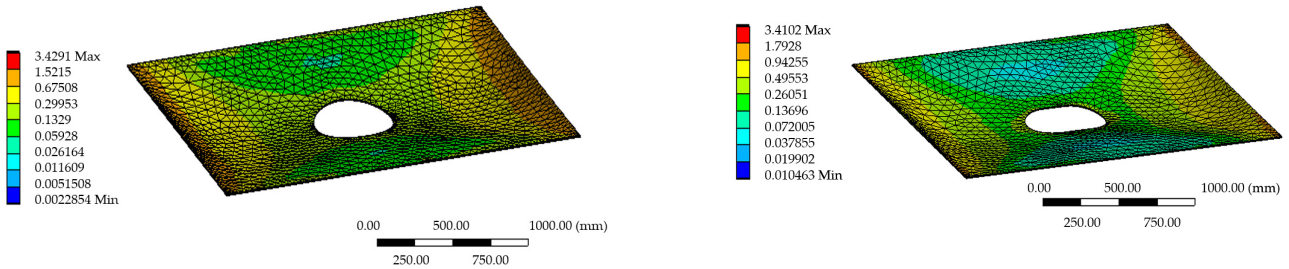

(**a**) (**b**)

Figure 14. Difference between opening shapes (von Mises stress, MPa): (**a**) circular and (**b**) elongated circular.

The elastic buckling strength is found to differ by 2.1% when compared with the findings presented by Paik [26]. A comparison of the FEM and DIC calculation methods is also used to validate this circular opening. In order to achieve this, a plate with a hole in the middle is constructed and examined using the Ncorr® open source 2D MATLAB® software (v1.2.2) [35], adhering to the same methodology as Kumar et al. [36]. This is then compared with its corresponding numerical analysis under the same design conditions, demonstrating a 1.87% difference between both regimes (Figure 15).

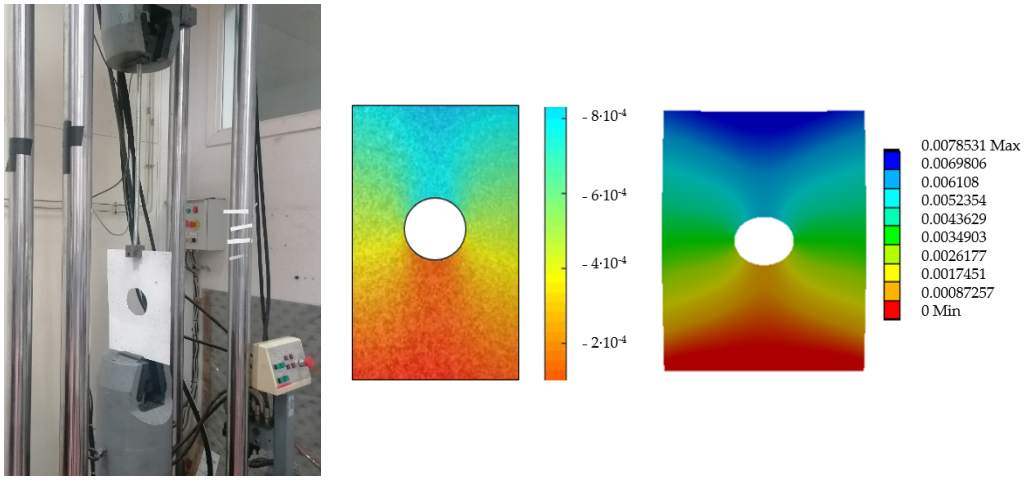

(**a**) (**b**)

Figure 15. Values for maximum displacement (in millimeters): (**a**) DIC and (**b**) FEM.

5. Results and Discussion

5.1. Tank Design for Sloshing Scenario

Sloshing and impact pressures due to liquid motion in the longitudinal or transverse direction is magnified by the resonance effect between the possible eigenfrequency coupling between the tank cargo and the vessel. Accordingly, and following the recommendations of Bureau Veritas [37] summarized in Table 7, a structural check of the tank is carried out.

Table 7. Resonance conditions as a function of tank and filling dimensions.

State	Risk of Resonance if 0.1 $H < d_F < 0.95\ H$	Resonance Due to
Upright	$0.6 < \frac{T_X}{T_{PITCH}} < 1.3, \frac{d_F}{l_C} > 0.1, T_X = \sqrt{\frac{4\pi l_S}{g \cdot \tanh \frac{\pi d_F}{l_S}}}$	Pitch
Heeled	$0.8 < \frac{T_Y}{T_{ROLL}} < 1.2, \frac{d_F}{b_C} > 0.1, T_Y = \sqrt{\frac{4\pi b_S}{g \cdot \tanh \frac{\pi d_F}{b_S}}}$	Roll

d_F is the level of water inside the tank whose weight is H, T_x is the natural period of the liquid motion in the longitudinal direction; T_{PITCH} is the pitch period of the vessel of scantling length L that can be approximated by the expression $T_{PITCH} = 0.575\sqrt{L}$; l_C is the longitudinal distance between transverse watertight bulkheads or transverse wash bulkheads; l_S is the length of the free surface of the liquid, measured horizontally with the ship at rest and depending on the filling level d_F; T_Y is the natural period of the liquid motion in the transverse direction; T_{ROLL} is the roll period of the vessel given by the expression $T_{ROLL} = 2.2\frac{0.35 \cdot B}{\sqrt{GM}}$, where the metacentric height GM is approximately by 0.07 B; b_c is the transverse distance between transverse watertight bulkheads or transverse wash bulkheads; and b_S is the breadth of the free surface of the liquid, measured horizontally with the ship at rest and depending on the filling level d_F.

5.2. Influence of Cutouts and Opening

The quantity and distribution of stresses and deformations surrounding the openings are determined by their geometry, location, number, and proximity, as well as the load conditions they undergo. The load multiplier factor (LMF) or buckling factor, an enhancing factor implemented in the design loading, indicates the critical buckling load. Under identical conditions, a lower LMF value corresponds with a lower critical buckling load and a negative growth in structural behavior. By estimating the value of the LMF and the maximum stress for each possible combination, a significant inverse relation between these two definitions is established, allowing one to ascertain how geometric discontinuities affect the buckling phenomenon (Figure 16).

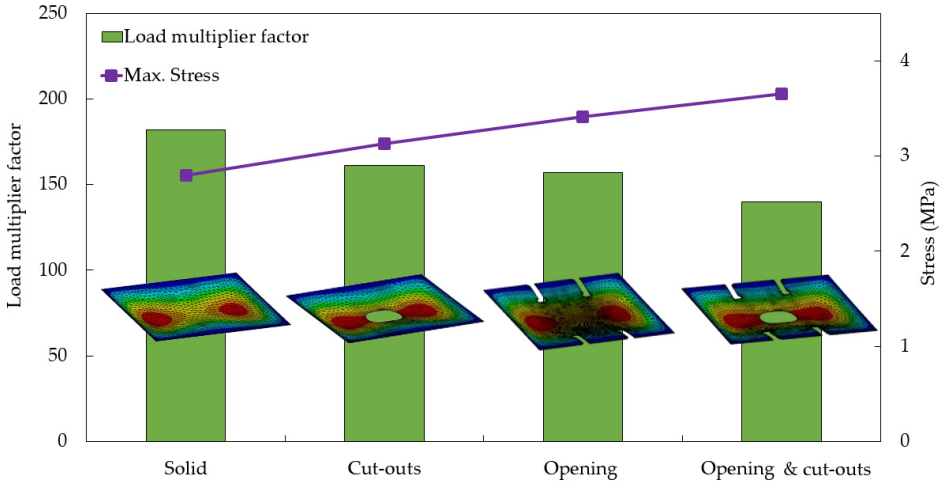

Figure 16. Contrast among models.

The geometric discontinuities directly affect the structural behavior, which translates into modifications of 9.23, 7.94, and 17.85% in terms of maximum displacement for plates with openings, plates with cutouts, and plates with both openings and cutouts, respectively. The superposition principle can be used to approach the effect of the opening, which is found to have a greater influence than the cutouts, because there is a linear combination between the two phenomena in terms of displacement value. There is a clear linear trend that can be further explored with a linear regression model. Table 8 provides more information about this model's coefficients.

Table 8. Linear regression model ($y = ax + b$).

	R^2	a	b
Stress	0.921	94.654	−1.226
Load multiplier factor	0.9805	−4561.1	375.46

In the regression model, x denotes the variable defining maximum deformation and y the variable to be predicted (load multiplier factor or maximum stress). The regression line's slope and intercept are denoted, respectively, by the coefficients a and b. The correlation coefficient (R^2) criterion is used to determine the strength of the linear relationship between the variables in order to evaluate the validity of the regression model. Regression line gradient analysis shows that, in comparison with stress, the load multiplier factor responds more readily to changes in deformation.

5.3. Evaluation of Plate Characteristics

By adjusting thickness according to the slenderness ratio, buckling can be reduced. The buckling modes of the perforated plate under two different thickness values and different load conditions are shown in Figure 17.

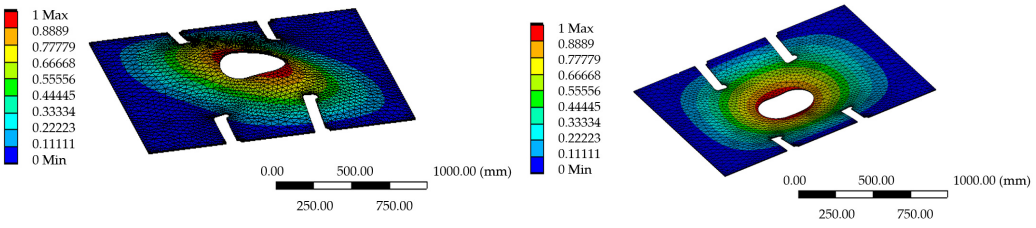

(**a**) (**b**)

Figure 17. Buckling collapse modes: (**a**) t = 12 mm and in-plane edge shear loading and (**b**) t = 10 mm and longitudinal compression.

Structural analyses are performed under different loading conditions (longitudinal, transverse, and biaxial compression) and thickness values, which are characterized by slenderness ratio, in order to assess the effect of increased thickness on improving performance. In order to strengthen the dependability of result extrapolation, two additional thickness values—18 mm and 20 mm—are introduced in this analysis (Figure 18).

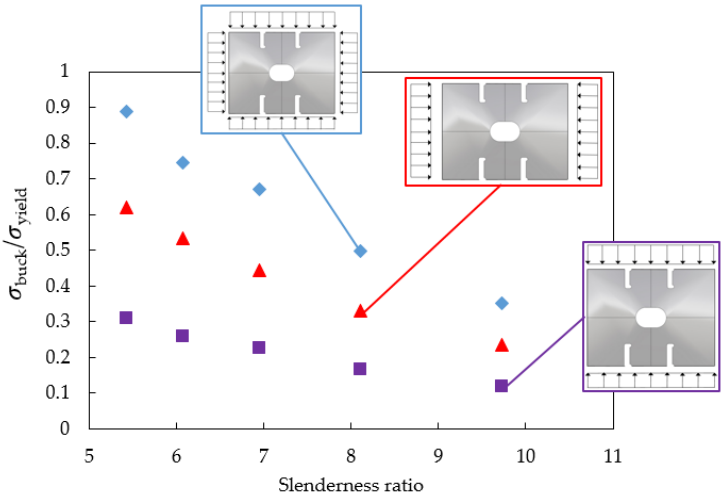

Figure 18. Normalized buckling critical stress for longitudinal, transverse, and biaxial compression based on the yield stress of the material in relation to the plate stiffness ratio.

Regardless of the load condition, a regular pattern in the structural response can be seen in the relationship between the ratios defining the plate slenderness and the normalized parameter ($\sigma_{buck}/\sigma_{yield}$). Among these, biaxial compression stands out as the least advantageous; the ratio value ($\sigma_{buck}/\sigma_{yield}$) differs from longitudinal and transverse compression by 30.3% and 65.1%, respectively.

5.4. Impact of Stiffening Technique

The addition of extra reinforcing elements is another way to increase buckling strength. Figure 19 compares the deformed shapes that occur when test specimens using different stiffening techniques are compressed longitudinally at varying sizes and in an elastic buckling framework.

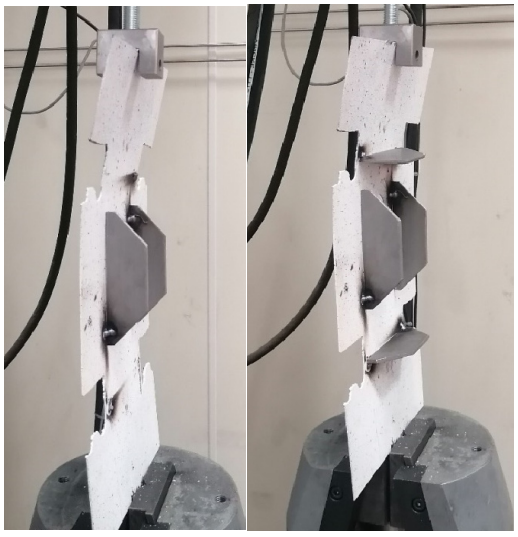

(**a**) (**b**)

Figure 19. Deformation pattern under longitudinal compression: (**a**) stiffening method c and (**b**) stiffening method b.

Improvements in maximum displacement can be obtained by adding reinforcement elements (as described in the different stiffening techniques presented in Figure 7). In comparison with the unstiffened perforated plate, improvements of 30.3%, 32.19%, 0.19%, and 9.61% are obtained with regard to stiffening methods a, b, c and d, respectively. The buckling modes associated with various stiffening methods, scantling variations and load scenarios are depicted in Figure 20.

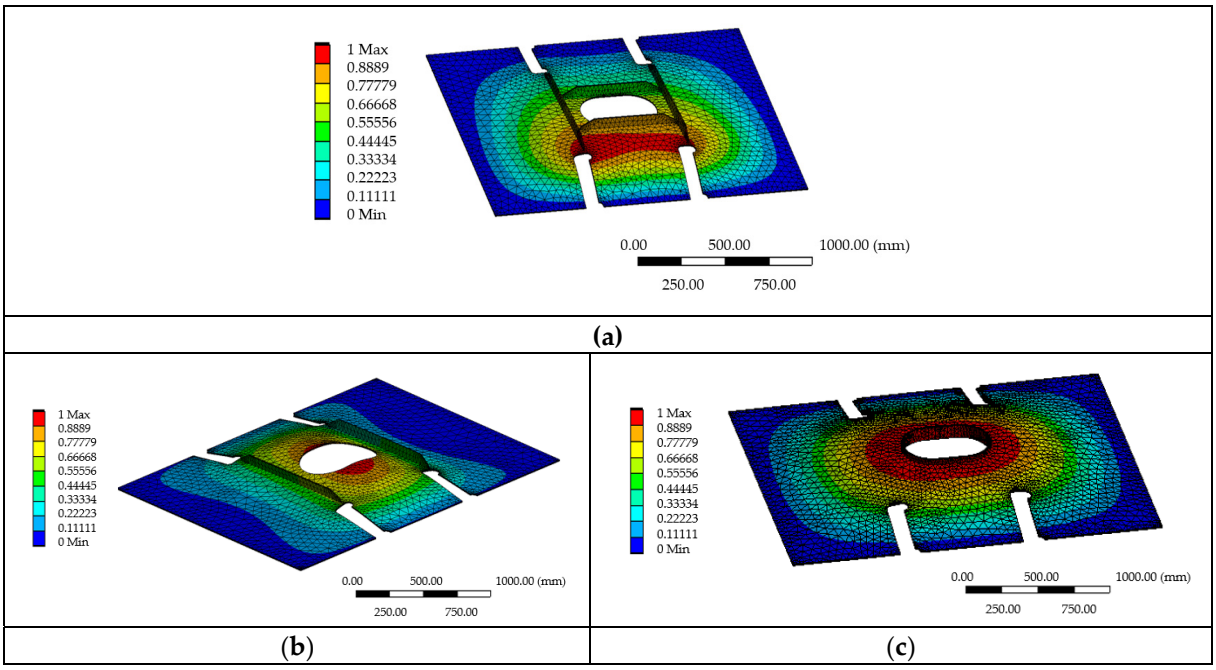

Figure 20. Buckling modes (mm): (**a**) Stiffening technique b80 × 12 (mm) under transverse compression, (**b**) stiffening technique a70 × 10 (mm) under longitudinal compression and (**c**) stiffening technique d80 × 14 (mm) under biaxial compression.

Figure 21 shows the evolution of the LMF value for the different types of reinforcement under conditions in relation to the biaxial loading condition.

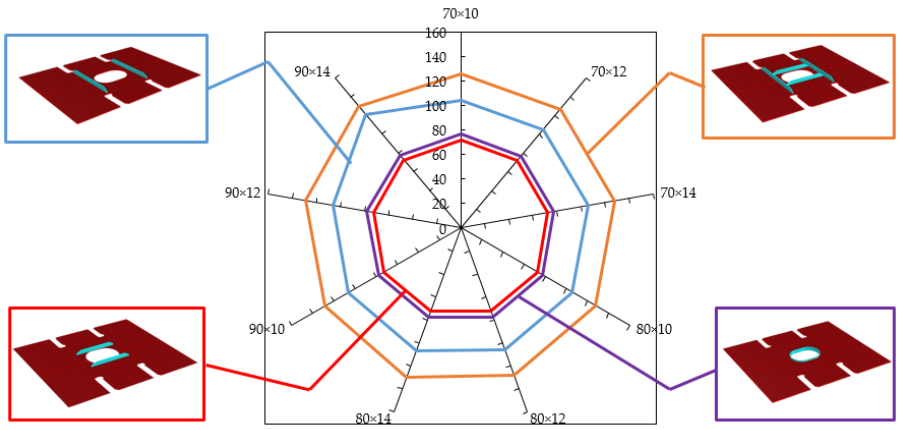

Figure 21. Progression of load multiplier factor (LMF) values relative to stiffening technique under biaxial compression.

Stiffening method *b* exhibits consistently better structural performance under all load conditions, outperforming stiffening method *a* by a small margin (approximately 9.76% for longitudinal compression). Furthermore, it performs significantly better than methods *c* (about 23.18% for longitudinal compression) and *d* (about 19.61% for longitudinal

compression), even though they are not identical. The main strategy for improving the buckling strength of the stiffened perforated plate is to increase the height and thickness of the stiffening flat bars. Different stiffening techniques respond differently to changes in the scantling dimensions. For example, in method *a*, regardless of flat bar height, a 16.66% increase in thickness results in a roughly 0.73% improvement in buckling strength. Similarly, irrespective of flat bar thickness, a 1% improvement is obtained with a 12.5% increase in height. In contrast, method b exhibits improvements in structural behavior that are highly dependent on the thickness value, ranging from a 1.85% enhancement regardless of flat bar height to a 16.66% enhancement when height is increased to 12.5%.

6. Conclusions

This comprehensive study undertook an extensive series of experimental tests and finite element analyses to thoroughly investigate and understand the elastic buckling behavior of perforated plates. These plates were characterized by a variety of openings and were subjected to different stiffening techniques under the influence of combined in-plane loads.

The numerical simulations performed as part of this study have shown a high level of agreement with the experimental results, demonstrating their accuracy and reliability. The research meticulously quantified and clearly demonstrated the impact of geometric discontinuities, such as openings and cutouts, on the reduction of buckling strength. It was found that central openings had a more significant effect compared with cutouts, with a notable 2.4% difference in impact. The study went further to analyze non-linear effects by examining the combined structural response of openings and cutouts together, rather than considering their individual impacts in isolation. This combined response was represented by the load multiplier factor, providing deeper insights into the complex interactions at play.

Additionally, the study revealed that increasing the thickness of the plate, as indicated by the slenderness ratio, directly enhances the buckling strength. This relationship between plate thickness and buckling strength can be assessed and extrapolated in a linear manner, irrespective of the specific load conditions. The implementation of various stiffening techniques was also explored, and it was found that these techniques yielded significantly better structural outcomes compared with simply increasing the thickness of the perforated plate alone. Specifically, the stiffening method identified as *b* resulted in a remarkable 19% improvement in buckling strength. In contrast, method *a* demonstrated a 14.1% improvement. Among the different stiffening techniques evaluated throughout the study, method *b* emerged as the most effective. This method provided the greatest enhancement in buckling strength while having a minimal impact on the weight of the structure, making it superior to the second most effective method.

Overall, this study provides valuable insights into the optimization of perforated plates, offering practical recommendations for improving their structural performance under various loading conditions. Further studies will consider the use of non-linear FEM analysis for determining the ultimate strength of the floor panel as a function of the geometric, rigidity and stiffening parameters considered in this study.

Author Contributions: Conceptualization, A.S.-C. and F.P.-A.; methodology, A.S.-C. and F.P.-A.; software, A.S.-C.; validation, F.P.-A.; formal analysis, A.S.-C. and F.P.-A.; investigation, A.S.-C. and F.P.-A.; resources, A.S.-C.; data curation, F.P.-A.; writing—original draft preparation, A.S.-C.; writing—review and editing, F.P.-A.; visualization, A.S.-C. and F.P.-A.; supervision, F.P.-A.; project administration, A.S.-C. and F.P.-A. All authors have read and agreed to the published version of the manuscript.

Funding: This research received no external funding.

Institutional Review Board Statement: Not applicable.

Informed Consent Statement: Not applicable.

Data Availability Statement: All data are presented in the paper.

Acknowledgments: The authors would like to acknowledge the support received from the Universidad Politécnica de Madrid.

Conflicts of Interest: The authors declare no conflict of interest.

References

1. Kawasaki, Y.; Okada, T.; Kobayakawa, H.; Amaya, I.; Miyashita, T.; Nagashima, T.; Neki, I. A study of forced vibration of double bottom structure due to whipping on an ultra large container ship. In Proceedings of the ASME 36th International Conference on Ocean, Offshore and Arctic Engineering, Trondheim, Norway, 25–30 June 2017. OMAE2017-61149. [CrossRef]
2. Bureau Veritas Rules. Structural Rules for Container Ships. NR625 DT R04 E. 2021. Available online: https://marine-offshore.bureauveritas.com/nr467-rules-classification-steel-ships (accessed on 14 April 2024).
3. Wang, G.; Sun, H.; Peng, H.; Uemori, R. Buckling and ultimate strength of plates with openings. *Ships Offshore Struct.* **2009**, *4*, 43–53. [CrossRef]
4. Liu, B.; Gao, L.; Ao, L.; Wu, W. Experimental and numerical analysis of ultimate compressive strength of stiffened panel with openings. *Ocean Eng.* **2021**, *220*, 108453. [CrossRef]
5. Saad-Eldeen, S.; Garbatov, Y.; Guedes Soares, C. Structural capacity of plates and stiffened panels of different materials with opening. *Ocean Eng.* **2018**, *167*, 45–54. [CrossRef]
6. Yanli, G.; Xiaoqing, S.; Xiao, L.; Xingyou, Y.; Zhifan, X.; Bin, X.; Jianyi, S. Elastic buckling of thin plate with circular holes in bending. *E3S Web Conf.* **2019**, *136*, 04043. [CrossRef]
7. Saad-Eldeen, S.; Garbatov, Y.; Guedes Soares, C. Experimental compressive strength analyses of high tensile steel thin-walled stiffened panels with a large lightening opening. *Thin-Walled Struct.* **2017**, *113*, 61–68. [CrossRef]
8. Kim, J.; Jeom, J.; Park, J.; Seo, H.; Ahn, H.; Lee, J. Effect of reinforcement on buckling and ultimate strength of perforated plates. *Int. J. Mech. Sci.* **2015**, *92*, 194–205. [CrossRef]
9. Chichi, D.; Garbatov, Y. Retrofitting analysis of tanker ship hull structure subjected to corrosion. *Brodogradnja* **2019**, *70*, 87–109. [CrossRef]
10. Cui, J.; Wang, S. An experimental and numerical investigation on ultimate strength of stiffened plates with opening and perforation corrosion. *Ocean Eng.* **2020**, *205*, 107282. [CrossRef]
11. Saad-Eldeen, S.; Garbatov, Y.; Guedes Soares, C. Experimental strength assessment of thin steel plates with a central elongated circular opening. *J. Constr. Steel Res.* **2016**, *118*, 135–144. [CrossRef]
12. Saad-Eldeen, S.; Garbatov, Y.; Guedes Soares, C. Experimental investigation on the residual strength of thin steel plates with a central elliptic opening and locked cracks. *Ocean Eng.* **2016**, *115*, 19–29. [CrossRef]
13. Yu, C.; Lee, J. Ultimate strength of simply supported plate with opening under uniaxial compression. *Int. J. Nav. Archit. Ocean Eng.* **2012**, *4*, 423–436. [CrossRef]
14. Kumar, M.; Alagusundaramoorthy, P.; Sundaravadiveu, R. Ultimate strength of stiffened plates with a square opening under axial and out-of-plane loads. *Eng. Struct.* **2009**, *31*, 2568–2579. [CrossRef]
15. Li, X.; Zhu, Z.; Li, Y.; Chen, Q.; Zhang, X. Mechanical behaviour of composite ship structures with open-hole. *IOP Conf. Ser. Mater. Sci. Eng.* **2020**, *892*, 012033. [CrossRef]
16. Doan, V.; Liu, B.; Garbatov, Y.; Wu, W.; Guedes Soares, C. Strength assessment of aluminium and steel stiffened panels with openings on longitudinal girders. *Ocean Eng.* **2020**, *200*, 107047. [CrossRef]
17. Xu, M.; Yanagihara, D.; Fujikubo, M.; Guedes Soares, C. Influence of boundary conditions on the collapse behaviour of stiffened panels under combined loads. *Mar. Struct.* **2013**, *34*, 205–225. [CrossRef]
18. Kim, U.; Choe, I.; Paik, J. Buckling and ultimate strength of perforated plate panels under axial compression: Experimental and numerical investigations with design formulations. *Ships Offshore Struct.* **2009**, *4*, 337–361. [CrossRef]
19. Cui, J.; Wang, D. A study of ultimate strengths of typical longitudinals girders with openings in container ships. In Proceedings of the ASME, 37th International Conference on Ocean, Offshore and Arctic Engineering, Madrid, Spain, 17–22 June 2018. OMAE2018-77820. [CrossRef]
20. Paik, J.K. Ultimate strength of steel plates with a single circular hole under axial compressive loading along short edges. *Ships Offshore Struct.* **2007**, *2*, 355–360. [CrossRef]
21. Silva-Campillo, A.; Suárez-Bermejo, J.C.; Herreros-Sierra, M.A. Design recommendations for container ship side-shell structure under fatigue strength assessment. *Ocean. Eng.* **2022**, *245*, 110655. [CrossRef]
22. Andersen, M.R. Fatigue Crack Initiation and Growth in Ship Structures. Ph.D. Thesis, Department of Naval Architecture and Offshore Engineering, Technical University of Denmark, Kongens Lyngby, Denmark, 1998.
23. Silva-Campillo, A.; Suárez-Bermejo, J.C.; Herreros-Sierra, M.A.; de Vicente, M. Design methodology in transverse webs of the torsional box structure in an ultra large container ship. *Int. J. Nav. Archit. Ocean. Eng.* **2021**, *13*, 772–785. [CrossRef]
24. Timoshenko, S.P.; Gere, J.M.; Prager, W. *Theory of Elastic Stability*, 2nd ed.; McGraw-Hill Book Co.: New York, NY, USA, 1962.
25. Paik, J.K.; Thayamballi, A.K. *Ship-Shaped Offshore Installations. Design, Building, and Operation*; Cambridge University Press: New York, NY, USA, 2007.
26. Paik, J.K. *Ultimate Limit State Analysis and Design of Plated Structures*; Wiley: New York, NY, USA, 2018.

27. Bureau Veritas Rules. Part B, Ch 4, Sec 3. 2024. Available online: https://marine-offshore.bureauveritas.com/nr467-rules-classification-steel-ships (accessed on 14 April 2024).
28. Det Norse Veritas. Structural Design Principles. DNVGL-RU-SHIP, Pt 3 Ch3. 2017. Available online: https://rules.dnv.com/servicedocuments/dnvpm/ (accessed on 17 April 2024).
29. Senjanovic, I.; Catipovic, I.; Tomasevic, S. Coupled flexural and torsional vibrations of ship-like girders. *Thin-Walled Struct.* **2007**, *45*, 1002–1021. [CrossRef]
30. Juncher, J.; Mansour, A.; Smærup, A. Estimation of ship motions using closed-form expressions. *Ocean Eng.* **2004**, *31*, 61–85. [CrossRef]
31. Bureau Veritas Rules. Part B, Ch 5, Sec 3. 2024. Available online: https://marine-offshore.bureauveritas.com/nr467-rules-classification-steel-ships (accessed on 21 April 2024).
32. ASD Ship Design, B.V. Intact Stability Requirements for Tugs with Application to Fairplay 22. 2012. Available online: https://www.onderzoeksraad.nl/nl/media/attachment/2018/7/10/bijlage_11_rapport_asd.pdf (accessed on 27 April 2024).
33. Paik, J.K.; Ham, J.H.; Kim, E.N. A new plate buckling design formula. *J. Soc. Nav. Archit. Jpn.* **1992**, *6*, 267–274. [CrossRef] [PubMed]
34. Patil, H.; Jeyakarthikeyan, P.V. Mesh convergence study and estimation of discretization error of hub in clutch disc with integration of ANSYS. *IOP Conf. Ser. Mater. Sci. Eng.* **2018**, *402*, 012065. [CrossRef]
35. Blaber, J.; Adair, B.; Antoniou, A. Ncorr: Open-Source 2D Digital Image Correlation Matlab Software. *Exp. Mech.* **2015**, *55*, 1105–1122. [CrossRef]
36. Kumar, S.; Aravind, H.; Hossiney, N. Digital image correlation (DIC) for measuring strain in brick masonry specimen using Ncorr open source 2D MATLAB program. *Results Eng.* **2019**, *4*, 1000061. [CrossRef]
37. Bureau Veritas Rules. Part B, Chapter 11, Sec 4, Page 438. 2024. Available online: https://marine-offshore.bureauveritas.com/nr467-rules-classification-steel-ships (accessed on 30 April 2024).